Journal of ELECTRONIC MATERIALS, Vol. 47, No. 10, 2018
https://doi.org/10.1007/s11664-018-6488-y

Piezoelectric, Dielectric and Ferroelectric Properties of $(1-x)(K_{0.48}Na_{0.52})_{0.95}Li_{0.05}Nb_{0.95}Sb_{0.05}O_3$-$x$ $Ba_{0.5}(Bi_{0.5}Na_{0.5})_{0.5}ZrO_3$ Lead-Free Solid Solution

BRENDA CARREÑO-JIMÉNEZ,[1] ARMANDO REYES-MONTERO,[2] M.E. VILLAFUERTE-CASTREJÓN,[2] and RIGOBERTO LÓPEZ-JUÁREZ[1,3]

1.—Unidad Morelia del Instituto de Investigaciones en Materiales, Universidad Nacional Autónoma de México, Antigua Carretera a Pátzcuaro No. 8701, Col. Ex Hacienda de San José de la Huerta, C.P. 58190 Morelia, Michoacán, Mexico. 2.—Instituto de Investigaciones en Materiales, Universidad Nacional Autónoma de México, Ciudad Universitaria, A.P. 70-360, C.P. 04510 CDMX, Mexico. 3.—e-mail: rlopez@iim.unam.mx

The lead-free solid solution $(1-x)(K_{0.48}Na_{0.52})_{0.95}Li_{0.05}Nb_{0.95}Sb_{0.05}O_3$-$xBa_{0.5}(Bi_{0.5}Na_{0.5})_{0.5}ZrO_3$ [KNLNS-xBBNZ] with $0.02 < x < 0.05$ was successfully prepared by a conventional solid-state route. The effect of BBNZ on the KNLNS phase structure, microstructure and electrical properties was investigated. X-ray diffraction patterns demonstrated a single-phase perovskite-type structure and for $0.02 < x < 0.03$ a rhombohedral–tetragonal (R–T) phase coexistence. In addition, the average crystal size greatly decreased with BBNZ doping. Furthermore, the piezoelectric and ferroelectric properties of the KNLNS-xBBNZ ceramics were enhanced at $x = 0.02$ (d_{33} = 292 pC/N, $-d_{31}$ = 100 pC/N, k_p = 48%, ε_r = 5876, $\tan\delta$ = 0.03) due to a high polarizability at a local level. For $x = 0.02$, the solid solution showed good thermal stability of the d_{33} piezoelectric constant. As a result, this lead-free solid solution holds potential for applications in electric generators and high-temperature sensors.

Key words: Lead-free piezoceramics, solid-state route, piezoelectric properties, phase coexistence

INTRODUCTION

The 'state of the art' in the synthesis, processing and electrical properties of lead-free ceramics reveals that doped potassium–sodium niobate (KNN) materials are the most promising candidates to replace lead zirconate-titanate (PZT) materials. Recent studies have reported that KNN-based materials have piezoelectric properties that are similar—and sometimes superior—to those of PZT-based ceramics.[1–5] The high d_{33} and $-d_{31}$ values, together with a good electromechanical coupling factor (k_p) and high Curie temperature (T_C) make these compositions suitable for applications such as high-temperature sensors, actuators and generators.

The enhanced piezo-ferroelectric properties of these compositions arise from the coexistence of rhombohedral–tetragonal (R–T) or rhombohedral–orthorhombic–tetragonal (R–O–T) phases as reported elsewhere.[6–8] The polymorphic phase transition (PPT) or phase coexistence, improves the electrical behaviour of these materials, although most of them are highly temperature dependent. Consequently, thermal stability is a critical issue that must be considered during the design of electronic devices.[9,10]

Most studies investigating the synthesis of KNN ceramics highlight the difficulty associated with achieving high-density materials lacking impurity

(Received April 23, 2018; accepted June 27, 2018; published online July 11, 2018)

phases.[10] Accordingly, a variety of synthesis methods have been tested, including sol–gel, hydrothermal, microwave-hydrothermal and conventional solid-state reactions.[11–17] In terms of practical use, the conventional solid-state reaction represents a low-cost method, given that carbonates and oxide reagents are inexpensive.

On the other hand, there are few reports concerning the final technological applications of lead-free KNN ceramics.[18–22] Some of the above mentioned drawbacks are related to the thermal stability and the presence of impurity phases. Both issues have influenced the final electric performance. In this work, the synthesis and piezo-ferroelectric properties of KNLNS-*x*BBNZ ceramics are reported, with special emphasis on the thermal stability of their piezoelectric properties.

EXPERIMENTAL PROCEDURE

Powder Preparation and Sintering

Ceramics with $1 - x(K_{0.48}Na_{0.52})_{0.95}Li_{0.05}Nb_{0.95}Sb_{0.05}O_3$-$xBa_{0.5}(Bi_{0.5}Na_{0.5})_{0.5}ZrO_3$ (KNLNS-*x*BBNZ) (x = 0, 0.02, 0.025, 0.03, 0.035, 0.04, 0.045 and 0.05) compositions, were prepared by conventional solid-state reaction from the adequate mixture of oxides and carbonates. Na_2CO_3 (Merck, 99.9%), Li_2CO_3 (Sigma-Aldrich, 99.99%), K_2CO_3 (JT Baker, 99.8%), $BaCO_3$ (Sigma-Aldrich, 99%), Nb_2O_5 (Sigma-Aldrich, 99.99%), ZrO_2 (Sigma-Aldrich, 99%), Bi_2O_3 (Sigma-Aldrich, 99.9%) and Sb_2O_5 (Sigma-Aldrich, 99.99%) were used as starting raw materials. Reagents were dried at 170°C for 4 h to eliminate the adsorbed moisture before being used. They were then weighed and mixed using acetone. The mixture was calcined at 850°C for 3 h. Afterwards, the powders were ball milled in a plastic jar with zirconia grinding media for 12 h in ethanol and dried at 120°C for 4 h. Samples 13 mm in diameter and 2 mm thick were uniaxially pressed at 260 MPa and sintered between 1120°C and 1180°C for 4 h. The samples required different sintering temperatures to obtain optimal properties because the studied solid solutions have different melting points. Moreover, the density of the sintered samples was determined using the Archimedes method.

Structural and Microstructural Analysis

The sintered pellets were analyzed to identify the crystalline phases by x-ray diffraction (XRD) using a Bruker D8 Advance diffractometer (Bruker AXS GmbH, Karlsruhe, Germany; CuK_α radiation, λ = 1.5406 Å). The XRD patterns were recorded over an angular range of 20–80° (2θ) with 0.02° step size, using a working voltage and current of 40 kV and 40 mA, respectively. The samples were microstructurally characterized using a field emission scanning electron microscope (SEM; JEOL-J7600F, Tokyo, Japan).

Piezoelectric and Ferroelectric Properties

For the electrical measurements, samples were polished and silver electrodes were coated on both sides of the sintered samples and fired at 500°C for 30 min. Ceramics were polarized at room temperature under a 4 kV/mm *dc* electric field in a silicone oil bath for 30 min. The piezoelectric constant d_{33} was measured using a PiezoMeter (Piezotest, UK). The d_{31} and electromechanical coupling coefficient (k_p) were determined at room temperature by an iterative automatic method for analysis of complex impedance measurements.[23] The dielectric constant

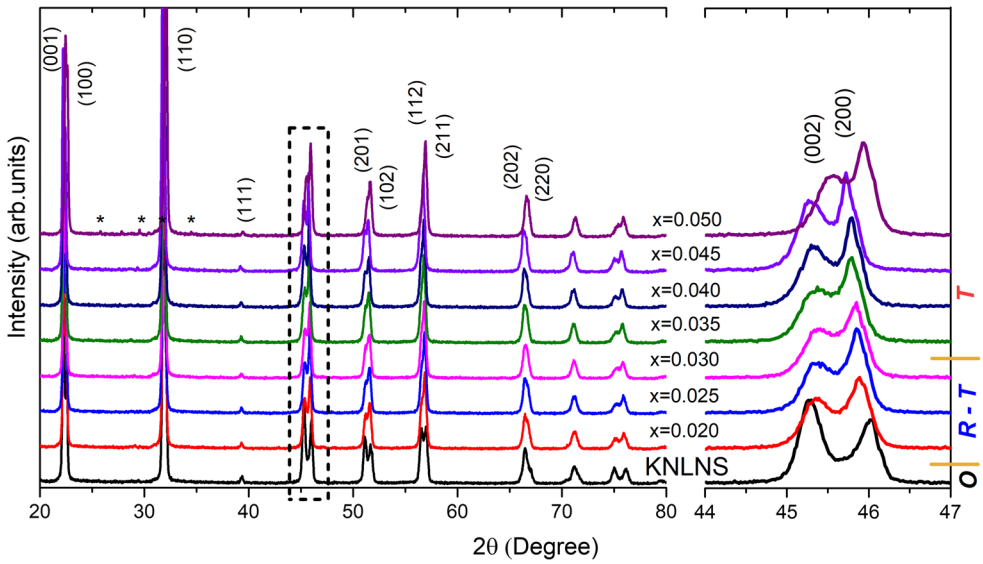

Fig. 1. XRD diffraction patterns of KNLNS-*x*BBNZ sintered ceramics between 20° and 80° (2θ), including a magnification of the (002/200) peak at 44.5–46.5° (2θ).

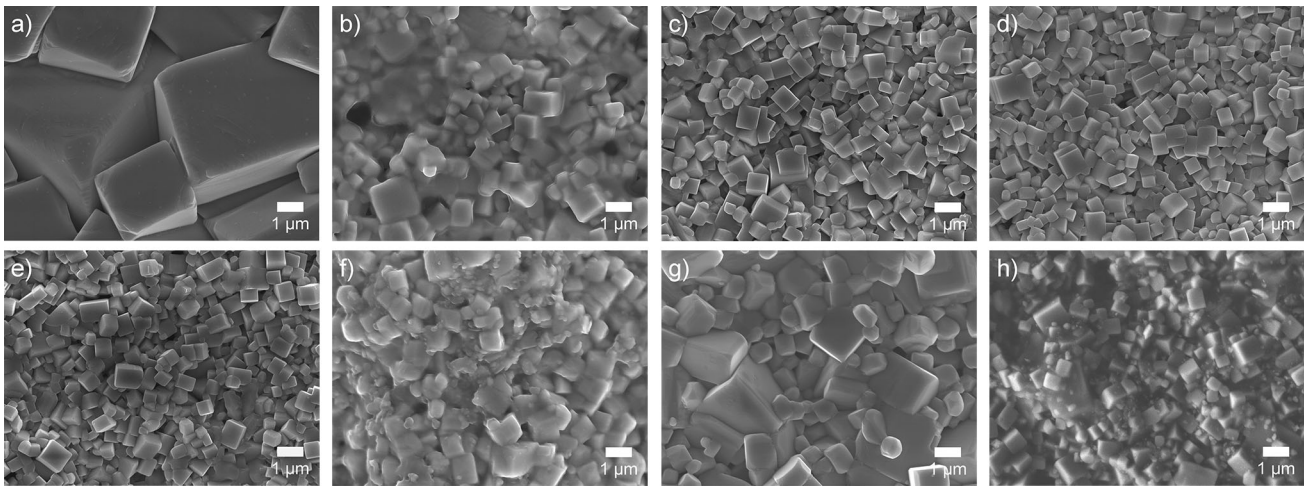

Fig. 2. SEM micrographs of KNLNS-*x*BBNZ sintered ceramic with x = (a) 0, (b) 0.02, (c) 0.025, (d) 0.03, (e) 0.035, (f) 0.04, (g) 0.045 and (h) 0.05.

Table I. Piezoelectric properties and average crystal size of KNLNS-*x*BBNZ and pure KNLNS sintered ceramics

Composition (x)	d_{33} (pC/N)	$-d_{31}$ (pC/N)	k_p (%)	ε_r (max)	Grain size (μm)
0	242	72	42	6064	4.6
0.020	292	100	48	5876	0.8
0.025	276	103	44	5375	0.6
0.030	275	94	44	5480	0.7
0.035	271	96	42	5326	0.5
0.040	266	90	41	5774	0.5
0.045	246	76	34	5872	0.3
0.050	236	78	34	4911	0.2

was determined at different temperatures using an impedance analyzer (Agilent 4294A, Santa Clara, CA, USA) at 100 kHz. Finally, the ferroelectric loops were acquired using a RT66B ferroelectric tester (Radiant Technologies, Albuquerque, NM, USA) at 100 Hz.

RESULTS AND DISCUSSION

The phase evolution of KNLNS-*x*BBNZ sintered pellets was characterized by XRD and the patterns are shown in Fig. 1. Most of the compositions revealed a pure perovskite structure indicating the formation of a solid solution, except for x = 0.045 and 0.05, where the solubility limit is reached. The observed impurity is typical in these materials[24] and consists of $K_3Li_2Nb_5O_{15}$ with a tungsten bronze structure.[25] A magnification around 45° (002 and 200 reflections) is also plotted in Fig. 1. This gives a clearer picture of the phase transition that occurs with the addition of BBNZ. For pure KNLNS, the crystal structure reveals an orthorhombic (O) phase due to the higher intensity of the 002 peak compared with the 200 reflection. For the $0.02 < x < 0.03$ compositions, the coexistence of tetragonal–rhombohedral (R–T) crystal structures is apparent. This is evident from the change in the 002/200 peak intensities. Furthermore, samples with $x > 0.03$ exhibited a dominant tetragonal (T) structure.[17]

In order to provide insight into the average crystal size and morphology of KNLNS-*x*BBNZ sintered samples, SEM images are shown in Fig. 2. The crystals have a cubic-like morphology, characteristic for these materials.[25,26] Moreover, the mean crystal size diminishes with an increase in BBNZ content. The average crystal size was measured using the *ImageJ* software and the results are shown in Table I. It can be observed that the average crystal size is between 0.8 and 0.2 μm as x increases from 0.02 to 0.05. Likewise, all samples exhibited a dense surface morphology including large and small grains. Therefore, a dense structure developed because smaller grains occupy the gaps among the larger ones, an important characteristic for enhancing the electrical properties of these materials.[1,27,28]

The ferroelectric loops measured at room temperature for KNLNS-xBBNZ ceramics are presented in Fig. 3a. The average coercive field (E_C), calculated from the positive and negative coercive fields, and the remnant polarization (P_r) are plotted in Fig. 3b. All samples show well-saturated P–E loops, representative of typical ferroelectrics. In addition, P_r increases with BBNZ content up to $x = 0.025$ and then slightly decreases. For the un-doped sample, P_r is close to 7.5 μC/cm^2, while compositions near the PPT approach 12 μC/cm^2. This behavior agrees with the XRD results, i.e. the polarization is maximum for samples located near the tetragonal–rhombohedral phase coexistence. On the other hand, the E_C remains between 12 kV/cm and 14 kV/cm. It is well-known that the presence of the PPT near room temperature implies an easier domain reorientation (i.e. remnant polarization enhancement) due to the existence of more possible orientation directions for the polarization vector.[17] This is directly correlated with improved dielectric and piezoelectric properties as discussed below.

The piezoelectric parameters for KNLNS-xBBNZ ceramics are presented in Table I. From the results, it is clearly observed that the highest piezoelectric properties were measured at $x = 0.02$. The d_{33} value reported in this work is larger than those reported in the KNN-based ceramic in other compositions.[29–32] This behavior corresponds with the crystallographic and ferroelectric characteristics. It is well known that there are 14 polarization directions (6-tetragonal, 8-rhombohedral) at the phase boundary which leads to high electrical performance.[33] The coexistence of both tetragonal and rhombohedral crystal structures contributes to the enhancement of piezoelectric performance due to the easy poling state of the samples. Figure 4 shows a representation of the complex impedance at resonance in the fundamental radial mode, of a thin disk, thickness poled ($t = 1$ mm and $D = 10.68$ mm) at room temperature. The peaks of the real part [resistance (R)] of the complex impedance (Z^*) and the real part [conductance (G)] of the complex admittance (Y^*) are used in the determination of some piezoelectric, dielectric and elastic material coefficients. From these data, the resonance and antiresonance frequencies, which are initial values for the iterative calculation of the piezoelectric parameters, were obtained. In our case, the experimental and the fitted data are in good agreement, indicating that the calculated parameters are highly reliable. The good fit of the $x = 0.02$ sample was mainly due to the density of the ceramic material obtained (free of internal defects), as well as the clear separation and intensity of the resonance/antiresonance peaks.[23]

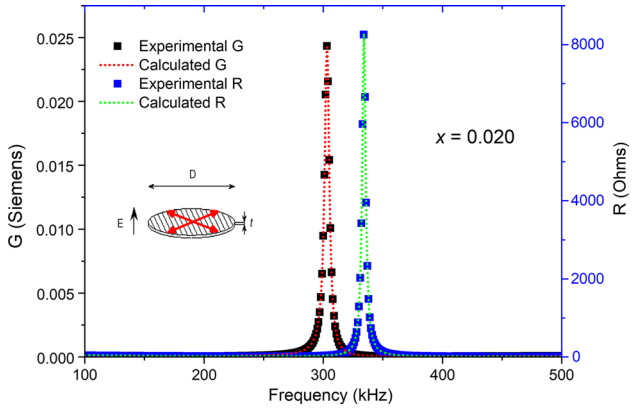

Fig. 4. R and G peaks, calculated at room temperature, for the fundamental radial mode of a thin disk ($t = 1$ mm and $D = 10.68$ mm).

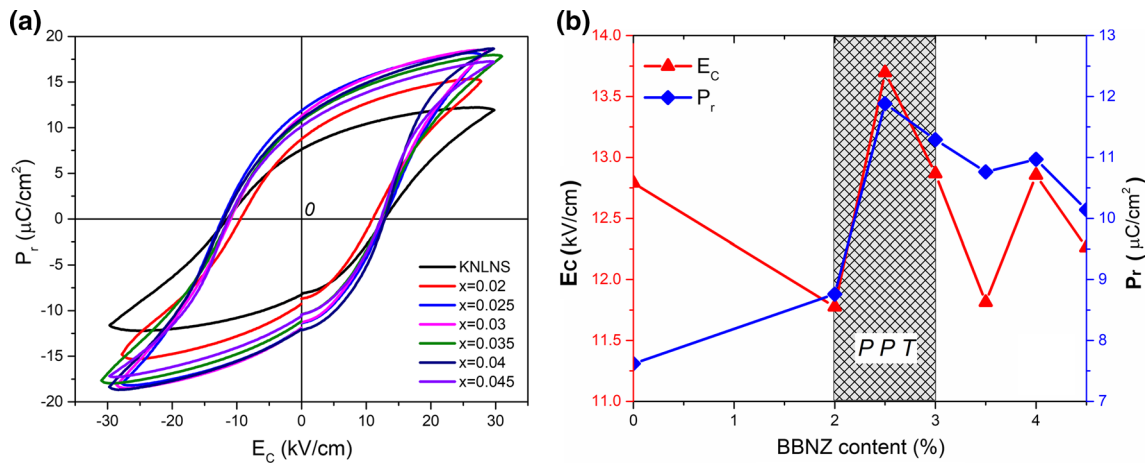

Fig. 3. (a) Ferroelectric hysteresis loops measured at room temperature for KNLNS-xBBNZ ceramics. (b) E_C and P_r values for different x content.

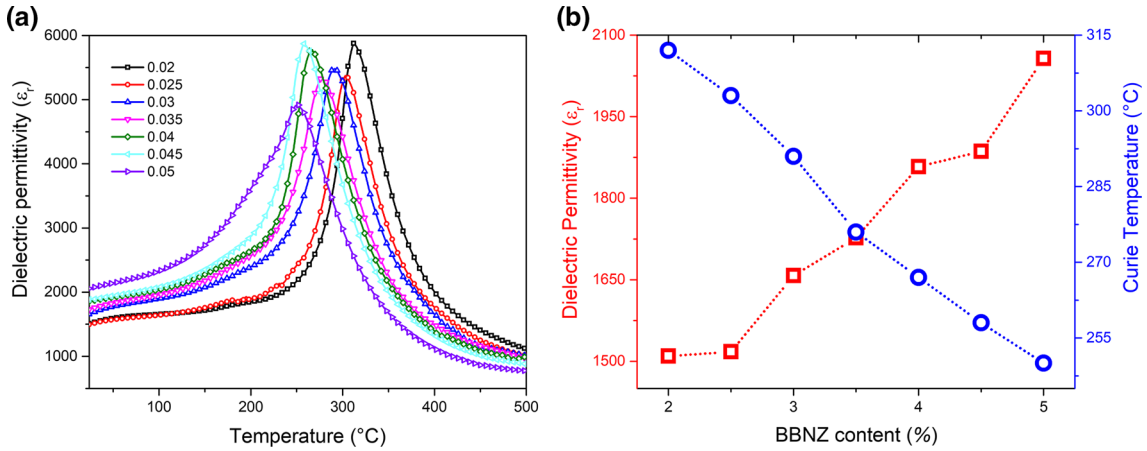

Fig. 5. (a) Dielectric permittivity measured at 1 kHz and (b) variations of ε_r and T_C for KNLNS-xBBNZ ceramics.

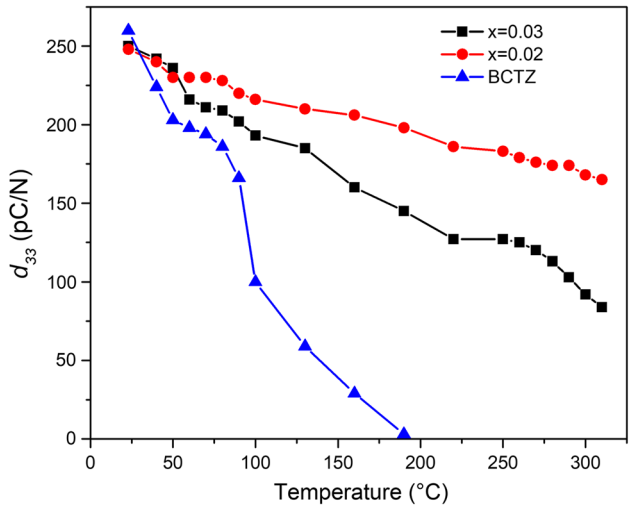

Fig. 6. Piezoelectric d_{33} constant versus temperature of KNLNS-xBBNZ (x = 0.02 and 0.03) and BCTZ sintered ceramics.

The dielectric permittivity (ε_r) for all KNLNS-xBBNZ samples is shown in Fig. 5. It is observed that upon increasing x both T_{O-T} and T_C shift to lower values, and T_{R-O} approaches room temperature when $0.02 < x < 0.03$. This could be attributed to the substitution of cations at the A and B sites of the perovskite structure. For example, Nb^{5+} has an ionic radius of 0.64 Å when it is sixfold coordinated while Zr^{4+} is 0.72 Å.[34] On the other hand, it is well known that $(Bi_{0.5}Na_{0.5})^{2+}$ and $BaZrO_3$ diminish both T_{O-T} and T_C.[7] Thus, the PPT construction close to room temperature enhances the ferroelectric, piezoelectric and dielectric properties as explained above. The permittivity or dielectric constant and the remnant polarization increase because of the R–T phase coexistence. Figure 5b demonstrates that doping of the B-site of the perovskite structure induces a shift of the T_C towards room temperature, which is mainly produced by lattice distortions.[3,8]

It is worth noting that the T_C remains high for all compositions, which prevents facile depolarization. Thus, samples with the best piezoelectric performance were exposed to a depolarization treatment to evaluate their piezoelectric stability. For comparison, a $Ba_{0.85}Ca_{0.15}Ti_{0.9}Zr_{0.1}O_3$ (BCTZ x = 0.15)[33,35] sample was also measured under the same characteristics.

The obtained results are shown in Fig. 6. The d_{33} piezoelectric constant remains high after the depolarization process at 200°C (~ 200 pC/N), and even after heating at 300°C, the d_{33} is around 60% of its initial value (~ 175 pC/N), while the properties of the BCTZ composition decreased by more than 70% when the sample was heated at 100°C (~ 100 pC/N). The depolarization process in piezo-ferroelectric ceramics gradually occurs due to a ferroelectric–ferroelectric phase coexistence, since the dipoles are slowly reoriented. This can explain the wide stability of the piezoelectric parameters. Therefore, the KNLNS-xBBNZ with x = 0.02 would be a suitable solid-solution for high-temperature sensor applications.

CONCLUSIONS

$(1-x)(K_{0.48}Na_{0.52})_{0.95}Li_{0.05}Nb_{0.95}Sb_{0.05}O_3$-$xBa_{0.5}(Bi_{0.5}Na_{0.5})_{0.5}ZrO_3$ lead-free solid solution piezoceramic was synthesized by a conventional solid-state method. The piezoelectric properties (d_{33} and k_p) for the bulk ceramics were maximum at x = 0.02 reaching 292 pC/N and 48%, respectively. The enhancement of piezoelectric properties is attributed to the coexistence of tetragonal and rhombohedral phases. A remarkable temperature stability for the electrical characteristics was observed. For x = 0.02 the d_{33} was close to 60% of its original value (even after thermal depolarization treatment at 300°C). These properties make the KNLNS-xBBNZ solid solution a suitable candidate for generators and high temperature sensors.

ACKNOWLEDGEMENTS

B. Carreño-Jiménez gratefully thanks CONACyT-México for providing a M.Sc. scholarship. The authors thank Omar Novelo (IIM-UNAM) and Neftalí Razo (ENES-Morelia) for SEM images and technical assistance, respectively. Also, to Federico González García and LDRX (T-128) UAM-I for XRD measurements. M. E. Villafuerte-Castrejón gratefully acknowledges PAPIIT-UNAM (IN109018) for financial support.

REFERENCES

1. L. Jiang, Y. Li, J. Xing, J. Wu, Q. Chen, H. Liu, D. Xiao, and J. Zhu, *Ceram. Int.* 43, 2100 (2017).
2. W. Wu, M. Chen, B. Wu, Y. Ding, and C. Liu, *J. Alloys Compd.* 695, 1175 (2017).
3. X. Wang, J. Wu, X. Cheng, B. Zhang, D. Xiao, J. Zhu, X. Wang, and X. Lou, *J. Phys. D Appl. Phys.* 46, 495305 (2013).
4. R. Zuo, X. Fang, and C. Ye, *Appl. Phys. Lett.* 90, 092904 (2007).
5. B. Wu, H. Wu, J. Wu, D. Xiao, J. Zhu, and S.J. Pennycook, *J. Am. Chem. Soc.* 138, 15459 (2016).
6. K. Zhang, Y. Guo, D. Pan, H. Duan, Y. Chen, H. Li, and H. Liu, *J. Alloys Compd.* 664, 503 (2016).
7. X. Tang, T. Chen, Y. Liu, J. Zhang, T. Zhang, G. Wang, and J. Zhou, *J. Alloys Compd.* 672, 277 (2016).
8. F. Rubio-Marcos, R. López-Juárez, R.E. Rojas-Hernández, A. del Campo, N. Razo-Pérez, and J.F. Fernandez, *ACS Appl. Mater. Interfaces.* 7, 23080 (2015).
9. K. Yoshida, K. Kakimoto, M. Weiß, S.J. Rupitsch, and R. Lerch, *Jpn. J. Appl. Phys.* 55, 10TD02 (2016).
10. X. Chen, G. Liu, G. Huang, X. Li, X. Yan, and H. Zhou, *J. Mater. Sci. Mater. Electron.* 28, 13126 (2017).
11. Y. Shiratori, A. Magrez, and C. Pithan, *J. Eur. Ceram. Soc.* 25, 2075 (2005).
12. D.Q. Zang, Z.C. Qin, X.Y. Yang, H.B. Zhu, and M.S. Cao, *J. Sol-Gel. Sci. Technol.* 57, 31 (2011).
13. N. Liu, K. Wang, J.F. Li, and Z. Liu, *J. Am. Ceram. Soc.* 92, 1884 (2009).
14. J.H. Lv, M. Zhang, M. Guo, W.C. Li, and X.D. Wang, *Int. J. Appl. Ceram. Technol.* 4, 571 (2007).
15. R. López-Juárez, R. Castañeda-Guzmán, and M.E. Villafuerte-Castrejón, *Ceram. Int.* 40, 14757 (2014).
16. W. Wu, M. Chen, B. Wu, Y. Ding, and C. Liu, *J. Alloys Compd.* 695, 2981 (2017).
17. Y. Zhao, Z. Xu, H. Li, J. Hao, J. Du, R. Chu, D. Wei, and G. Li, *J. Electron. Mater.* 46, 116 (2017).
18. I. Kanno, T. Ichida, K. Adachi, H. Kotera, K. Shibata, and T. Mishima, *Sens. Actuator A Phys.* 179, 132 (2012).
19. K.H. Lam, X.X. Wang, and H.L.W. Chan, *Sens. Actuator A Phys.* 125, 393 (2006).
20. A.G. Akyurekli, M. Gurbuz, M. Gul, H. Gulec, and A. Dogan, in *International Workshop on Acoustic Transduction Materials and Devices & Workshop on Piezoresponse Force Microscopy, Joint IEEE International Symposium on the Applications of Ferroelectric*, 2014.
21. E. Sapper, A. Gassmann, L. Gjødvad, W. Jo, T. Granzow, and J. Rödel, *J. Eur. Ceram. Soc.* 34, 653 (2014).
22. S.L. Yang, S.M. Chen, C.C. Tsai, C.S. Hong, and S.Y. Chu, *IEEE Trans. Ultrason. Ferroelectr. Freq. Control* 60, 408 (2013).
23. C. Alemany, A.M. González, L. Pardo, B. Jiménez, F. Carmona, and J. Mendiola, *J. Phys. D Appl. Phys.* 28, 945 (1995).
24. D. Lin, K.W. Kwok, and H.L.W. Chan, *J. Appl. Phys.* 102, 034102 (2007).
25. T.A. Skidmore and S.J. Milne, *J. Mater. Res.* 22, 2265 (2007).
26. R. López-Juárez, F. González-García, J. Zárate-Medina, R. Escalona-González, S. Díaz de la Torre, and M.E. Villafuerte-Castrejón, *J. Alloys Compd.* 509, 3837 (2011).
27. B. Wu, J. Wu, D. Xiao, and J. Zhu, *Dalton Trans.* 44, 21141 (2015).
28. W. Wu, M. Chen, J. Li, Y. Ding, and C. Liu, *J. Alloys Compd.* 670, 128 (2016).
29. J. Kim and J.H. Koh, *Ceram. Int.* 43, S92 (2017).
30. B. Zhang, X. Wang, X. Cheng, J. Zhu, D. Xiao, and J. Wu, *J. Alloys Compd.* 581, 446 (2013).
31. H. Li, W.Y. Shih, and W.H. Shih, *J. Am. Ceram. Soc.* 90, 3070 (2007).
32. D.W. Wu, R.M. Chen, Q.F. Zhou, K.K. Shung, D.M. Lin, and H.L.W. Chan, *Ultrasonics* 49, 395 (2009).
33. A. Reyes-Montero, L. Pardo, R. López-Juárez, A.M. González, S.O. Rea-López, M.P. Cruz, and M.E. Villafuerte-Castrejón, *Smart Mater. Struct.* 24, 065033 (2015).
34. R.D. Shannon, *Acta Crystallogr. A* 32, 751 (1976).
35. A. Reyes-Montero, P. Ramos-Alvarez, A.M. González, R. López-Juárez, and M.E. Villafuerte-Castrejón, *Appl. Sci.* 7, 214 (2017).